The Seybold Report
ISSN 1533-9211
DOI: 10.5281/zenodo.14598815

IMPACT BEHAVIOUR OF COIR FIBER/EPOXY COMPOSITE LAMINATES UNDER LOW-VELOCITY LOADING: A STUDY ON IMPACT BEHAVIOUR AND DAMAGE TOLERANCE

ENOCK A. DUODU*

Department of Mechanical and Automotive Engineering, Akenten Appiah-Menka University of Skills Training and Entrepreneurial Development, Ghana. *Corresponding Author Email: eaduodu@aamusted.edu.gh

Abstract

Natural fibers, such as coir, have gained significant attention as reinforcements in composite materials due to their sustainability and cost-effectiveness. This study numerically investigates the mechanical behavior of coir fiber/epoxy composite laminates subjected to low velocity loading using finite element analysis (FEA) with the explicit dynamic solver in ABAQUS. Also, cohesive zone model (CZM) is employed to capture delamination initiation and propagation at ply interfaces, while the 3D Hashin-Rotem failure criterion is used to predict matrix cracking. Various ply configurations were examined to assess their impact resistance, focusing on energy absorption, delamination, and matrix cracking under impact loading. Results show that ply orientation significantly affects energy dissipation, with certain configurations demonstrating improved impact resistance due to better stress distribution and reduced delamination. The findings provide insight into the design of natural fiber composites for applications requiring robust impact resistance.

Keywords: Coir Fiber Composites, Low-Velocity Impact, 3D Hashin-Rotem Failure Criterion, Energy Absorption, Ply Orientation.

1. INTRODUCTION

The increasing demand for sustainable and eco-friendly materials in various industries has driven the exploration of natural fiber-reinforced composites as alternatives to conventional synthetic materials. Among these natural fibers, coir (derived from the husk of coconuts) has garnered attention due to its abundance, biodegradability, and favorable mechanical properties such as toughness, high lignin content, and resistance to microbial attacks. Coir fiber-reinforced composites, when combined with polymer matrices like epoxy, offer promising potential in structural applications, especially where environmental concerns are paramount[1] One critical area of application for fiber-reinforced composites is in structures subjected to dynamic or impact loading. Low-velocity impacts, such as those caused by tool drops or collisions, can induce significant internal damage in composites, often without visible surface deformation [2, 3]. The damage mechanisms in composites under impact include matrix cracking, delamination, and fiber breakage, all of which reduce the structural integrity of the material [4]. While considerable research has been conducted on synthetic fiber-reinforced composites like carbon and glass fibers, studies focusing on the impact behavior of natural fiber-reinforced composites, particularly coir, are still limited. Low-velocity impacts, such as accidental drops, pose a significant challenge to composite materials, often leading to internal damage such as matrix cracking, fiber breakage, and delamination [5] Delamination, in particular, is a critical failure mode that can significantly reduce the structural integrity of composite laminates.

ISSN 1533-9211 DOI: 10.5281/zenodo.14598815

Understanding the coir fiber/epoxy laminates respond to such impact conditions is critical for design optimization in automotive, aerospace, and manufacturing industries as well as sporting equipment. Most existing research on natural fiber composites [6-10] focuses on static mechanical properties such as tensile strength, flexural behavior, and thermal stability. However, the response of coir fiber composites to simulate impact loading, particularly on angle-ply configurations, remains underexplored. In this paper, a numerical approach is used to analyze the impact behavior and damage mechanism of coir fiber/epoxy composite laminates under low-velocity impact.

2. MODEL DEVELOPMENT

2.1 Intra-laminar damage

In the study, intra-laminar damage is envisaged to occur, and accordingly, constitutive laws are required to trigger damage initiation and propagation. The failure modes are established and executed in ABAQUS/Explicit solver through the user-defined material subroutine. Thus, 3D Hashin-Rotem failure criterion in reference [11, 12] is adopted to simulate intra-layer fiber and matrix failures, and described as follows:

Matrix tensile failure

$$\left(\frac{\sigma_2}{Y_t}\right)^2+\left(\frac{\tau_{12}}{S_{12}}\right)^2+\left(\frac{\tau_{23}}{S_{23}}\right)^2=1 \qquad (1)$$

Matrix compressive failure

$$\frac{\sigma_2}{Y_c}-1+\left(\frac{\tau^2_{12}}{S^2_{12}}\right)^2+\left(\frac{\tau^2_{13}}{S^2_{13}}\right)^2=0 \qquad (2)$$

Fiber tensile failure

$$\left(\frac{\sigma_1}{X_t}\right)^2+\left(\frac{\tau_{12}}{S_{12}}\right)^2+\left(\frac{\tau_{13}}{S_{13}}\right)^2=1 \qquad (3)$$

Fiber compressive failure

$$\frac{\sigma_1}{X_c}=1 \qquad (4)$$

Where $\sigma_1,\sigma_2,\sigma_3$ are the normal stresses in longitudinal, transverse, and thickness directions, respectively. $\tau_{12},\tau_{13},\tau_{23}$ Show respective shear stresses (in-plane, out-of-plane, and through-thickness directions). X_t, X_c, Y_t, Y_c Are the respective strengths (fiber longitudinal tensile, fiber longitudinal compressive, matrix transverse tensile, matrix transverse compressive).

The Seybold Report
ISSN 1533-9211
DOI: 10.5281/zenodo.14598815

S_{12}, S_{13}, S_{23} Denote allowable shear strengths (in-plane, out-of-plane, and through-thickness) directions, respectively.

2.2 Inter-laminar damage

Inter-laminar damage in stiffened composite panel is very complex phenomenon during initiation and growth regimes; consequently, cohesive zone model is established via integrated mixed-mode criterion to stimulate the damage initiation threshold. A cohesive interface model based on quadratic strain interaction criterion (Eq. 5) is employed as defined in reference [13].

$$\left(\frac{\langle \delta_n \rangle}{\delta_n^0}\right)^2 + \left(\frac{\delta_s}{\delta_s^0}\right)^2 + \left(\frac{\delta_t}{\delta_t^0}\right)^2 \geq 1 \qquad (5)$$

δ_n^0, δ_s^0 and δ_t^0 denote the normal and shear direction of contact separation peak values, with corresponding δ_n, δ_s and δ_t separation mode displacements. To describe the normal and shear separation damage evolution along the interface, an effective separation δ_m is incorporated into the model as expressed below;

$$\delta_m = \sqrt{\langle \delta_n \rangle^2 + \delta_s^2 + \delta_t^2} \qquad (6)$$

Delamination growth under mixed mode loading based on B-K energy fracture criterion detailed in reference [13] is used.

$$G^c = G_n^c + \left(G_s^c - G_n^c\right)\left(\frac{G_s^c + G_t^c}{G_s^c + G_n^c}\right)^\eta \qquad (7)$$

The normal and shear critical fracture energy in Eq. 7 is represented by G_n^c, G_s^c and G_t^c, respectively, G^c denotes fracture energy of delamination, with η as cohesive coefficient.

FORTRAN pre-compiler code involving these constraint equations is written and executed into the commercial explicit finite element software ABAQUS 2020 version through a user-coded material subroutine [14].

3. FINITE ELEMENT MODEL

3.1 Structural Parameters and Boundary Conditions

The numerical simulation was conducted using the commercial finite element software ABAQUS/explicit solver to model the low-velocity impact on coir/epoxy composite laminates. The composite laminate was modeled as a multilayer structure, with a thickness of 3 mm and diameter of 112 mm. The laminate consisted of four plies with varying fiber orientations: [0°/45°/-45°/90°], [30°/60°/-60°/120°], and [15°/45°/-45°/75°]. A low velocity impactor of mass 2 kg was dropped from a height of 1 m to achieve an impact energy of 19.62 J. The impactor was modelled as a rigid body, and contact between the impactor and the composite

ISSN 1533-9211 DOI: 10.5281/zenodo.14598815

laminate was defined using a penalty contact algorithm with frictionless conditions. Constrained boundary conditions are fully apportioned along the circumference of the composite plate, with all DOFs restrained to zero to mimic experimental setup.

3.2 Element Size

The spherical impactor was meshed by the four-node rigid shell element (R3D4). In order to accurately resolve the strain gradients at the impact zone, a fine mesh of element size 0.5 mm^2 was used in the central patch surrounding the impact point. A fine mesh was generated using C3D8R hexahedral elements (8-node linear brick, reduced integration, and hourglass control) to model the composite laminate, and traction separation cohesive elements (COH3D8) of zero-thickness is also introduced between layers with different ply configurations to discretize the interface for debonding activation. The quadratic strain interaction criterion and B-K energy fracture law are used to predict damage initiation and propagation, whiles stress-based 3D Hashin-Rotem failure criterion is adopted for intra-laminar damage together with a continuum damage mechanics available in ABAQUS/Explicit software. A relative fine element mesh of 0.1 mm x 0.1 mm is applied on the impact location on the laminate. The mesh size was refined in the impact zone to ensure accurate capture of stress gradients; and failed interface elements were allowed to remain in the model to circumvent penetration of damage layers using an element option in ABAQUS/Explicit platform. A total number of 87640 solid elements, 79276 cohesive elements and 231420 nodes were applied for the simulation. Fig. 1 shows the finite element mesh of the spherical impactor and the laminated composite plate.

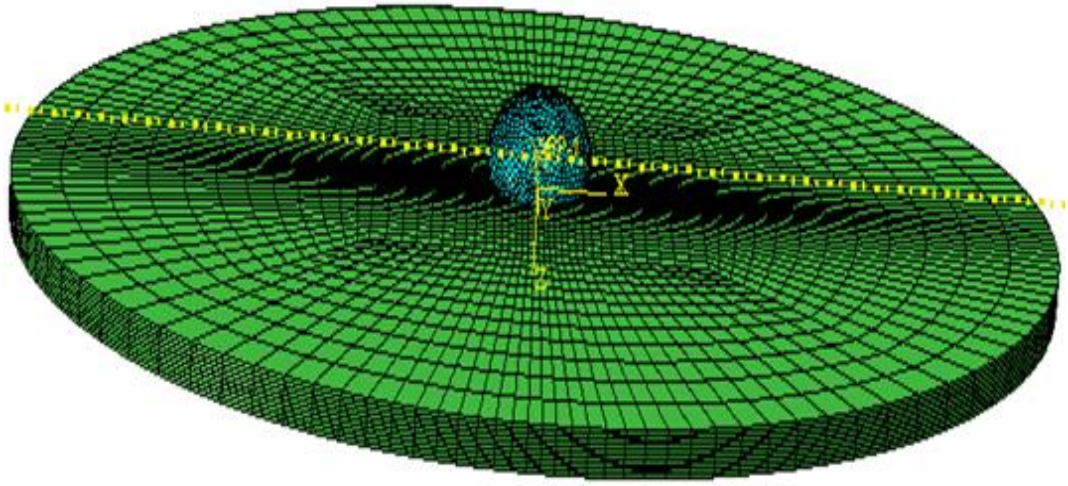

Figure 1: FE model of coir/epoxy composite laminate

3.3 Contact and Material Properties

The interaction between the analytical rigid impactor and composite plate is actuated by surface-to-surface contact pairs within ABAQUS/Explicit platform with penalty enforcement contact method [15], and is applied to avoid arbitrary penetration. The material properties and cohesive parameters obtained from literature [16, 17] are listed in Table 1.

ISSN 1533-9211 DOI: 10.5281/zenodo.14598815

Table 1: Material properties and cohesive parameters used in the model analysis

Density		1350 kg/m^3
Laminate	Elastic properties Strength	E_{11} = 6 GPa; E_{22} = E_{33} = 3 GPa; ν_{12} = ν_{13} = 0.057; ν_{23} = 0.36 G_{12} = G_{13} = 1.15 GPa; G_{23} = 4.7 GPa X_t = 0.98 GPa; X_c = 10 GPa; Y_t = 0.044 GPa; Y_c = 0.285 GPa; S_{12} = 0.0606 MPa; S_{13} = 0.0606 GPa; S_{23} = 0.022 GPa
Cohesive element	Elastic properties Strength Fracture energy	$K_n = 4.16\times10^6$; $K_s = K_t = 7.041\times10^3$ N/mm^3 δ_n^0 = 60 MPa; $\delta_s^0 = \delta_t^0$ = 90 MPa G_{IC} = 1200 N/m^2; $G_{IIC} = G_{IIIC}$ = 3000 N/m^2; η = 2

3.4 Computational Procedure

The formulated constitutive model is executed in the material user subroutine compiled in FORTRAN, and linked with the commercial finite element solver in ABAQUS/Explicit. The diagram in Fig. 2 shows the computational flow process of the model. Throughout the computational process, ABAQUS/Explicit transfers information of strain increment to the subroutine (material properties, strain increment of the current increment step, time increment size as well as the state variables of the previous increment step such as strain and damage). When the material variables are entered and the failure benchmark is fulfilled, the homogenized-material properties reduction is performed to update the failed variables. The stresses/strains at the integration points of the elements are updated by the reduced stiffness matrix. The updated variables returned to ABAQUS/Explicit for next step of analysis to commence.

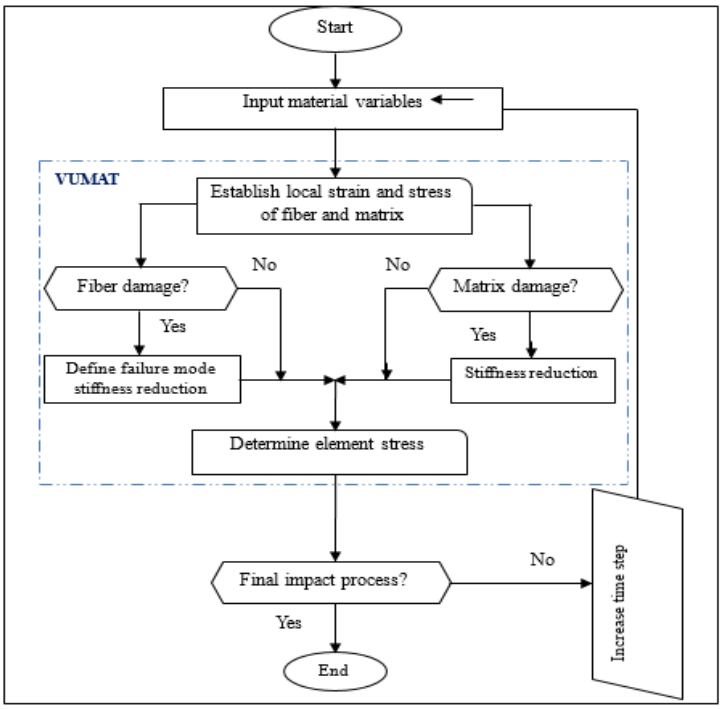

Figure 2: Flow diagram of computational impact process

ISSN 1533-9211 DOI: 10.5281/zenodo.14598815

4. RESULTS AND DISCUSSION

The numerical results are discussed to validate the applicability of the model. The impact tests were conducted on angle-ply coir fiber composite laminates with varying ply orientations, specifically [0°/45°/-45°/90°], [30°/60°/-60°/120°], and [15°/45°/-45°/75°] using impact energies ranged from 10 J to 40 J. This study focuses on the impact resistance and damage modes of coir fiber/epoxy composite laminates subjected to low velocity loading compared with the experimental data obtained from references.

4.1 Validation of Coir Fiber/Epoxy Composite Laminate

Numerical result obtained from the coir angle-ply of stacking sequence [0/45/-45/90] with initial velocity 0.2 m/s was applied to authenticate the applicability of the proposed model. In this model verification, two impact tests were performed; firstly, cohesive interface elements were introduced at each interface of fiber direction, thus, interfaces (1-3). During the examination, damage was found in all the three interfaces.

Additionally, numerical simulation and experimental test force as a variable of time was compared as shown in Fig. 3, and observably, simulation results and empirical findings were found to be in better accord with insignificant marginal model variance of 0.06, 3.2 and 3.7 % corresponding to impact energy levels of 3.14 6.28 and 15.7 J, respectively. The discrepancy may arise due to approximation of the failure criteria in the model.

In Figs. 2(a-c), maximum impact load of 1277, 1783 and 1786 were predicted for the three ascending energy regimes with corresponding impact energy levels, which agrees excellently with observation test values of 1265, 1841 and 1855 N, respectively.

Thus, the force-time curves from the simulation closely matched the experimental data, with a correlation coefficient of 0.95, validating the accuracy of the numerical models.

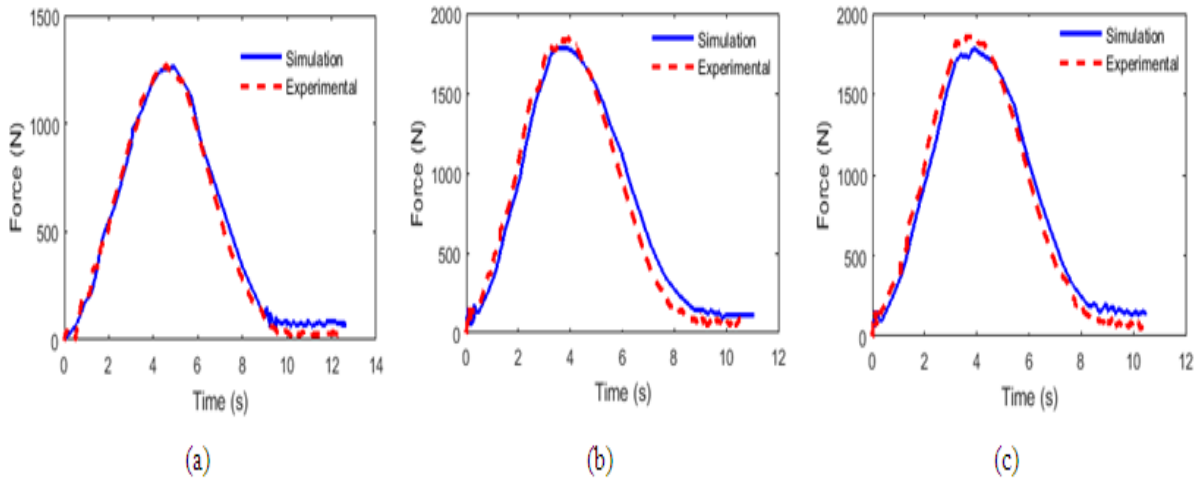

Figure 3: Impact force-time curves under different impact energy levels (a) 3.14 J (b) 6.28 J (d) (c) 15.7 J

ISSN 1533-9211 DOI: 10.5281/zenodo.14598815

4.2 Structural Response

4.2.1 Force-displacement analysis

Figure 4 shows the force-displacement curves for angle-ply coir fiber composite laminates under low-velocity impact loading provide critical insights into the material's impact behaviour. The three configurations analyzed exhibit distinct characteristics in response to impact test, as reflected in the plotted curves. Numerical result on [0°/45°/-45°/90°] laminate exhibited the highest peak force of 2500 N, followed by the [30°/60°/-60°/120°] laminate of 1650 N, and the [15°/45°/-45°/75°] laminate of 1800 N at 20 J. The force-displacement curves indicated that angle-ply laminates with higher angular orientations, thus, 45° absorbed more energy before failure compared to lower angles. This suggests that more uniform fiber orientations lead to better load distribution across the laminate, reducing stress concentrations and delaying failure initiation[18]

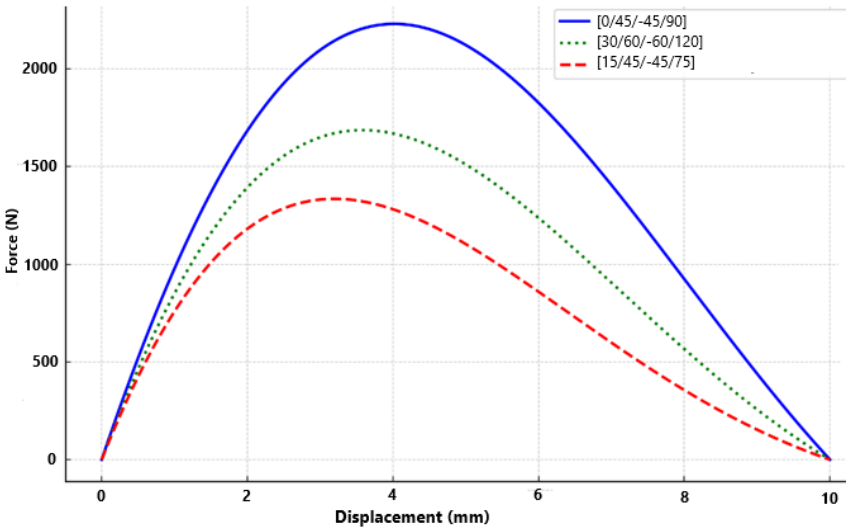

Figure 4: Force against Displacement for Angle-ply Coir Fiber Composite Laminates at 20 J Impact level

Again, the [0°/45°/-45°/90°] configuration absorbed more impact energy due to the more effective load transfer between the plies. In contrast, the [15°/45°/-45°/75°] laminate exhibited earlier onset of damage, followed with [30°/60°/-60°/120°] as indicated by the faster decline in the force-displacement curve after peak loading (Fig. 4).

4.2.2 Energy Absorption Rate

Energy absorption curves for the laminates revealed that the [0°/45°/-45°/90°] configuration could absorb 20% and 40 % more energy before the onset of significant damage compared to the [30°/60°/-60°/120°] and [15°/45°/-45°/75°] laminates, respectively. The cohesive zone model (CZM) used to simulate delamination showed that delamination initiated at lower energy levels in the [15°/45°/-45°/75°] configuration, particularly at the interfaces between 15° and 45° plies (Fig. 5).

ISSN 1533-9211 DOI: 10.5281/zenodo.14598815

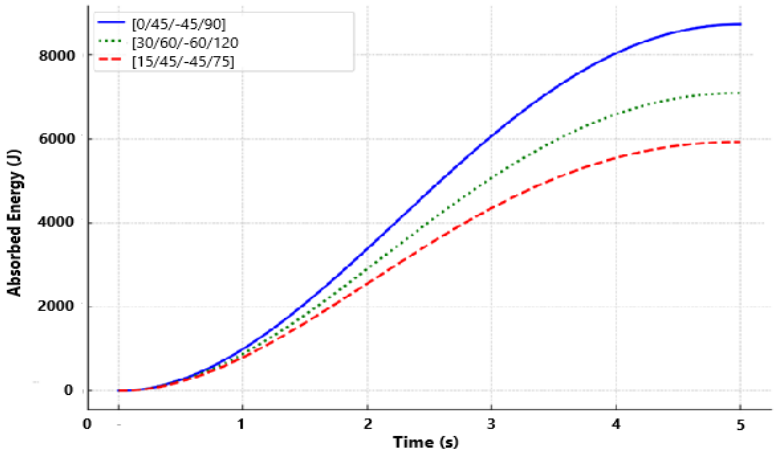

Figure 5: Absorption Energy with Time for Angle-ply Coir Fiber Composite Laminates at 20 J Impact Level

In all configurations, delamination was most severe at the ply interfaces with the largest angular differences. This aligns with previous studies indicating that larger angular discrepancies between fiber orientations increase interlaminar shear stresses, promoting delamination [19].

4.3 Damage Mechanisms

4.3.1 Matrix Cracking and Fiber Breakage

45°/-45°/90°]	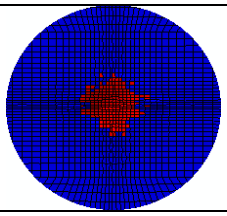	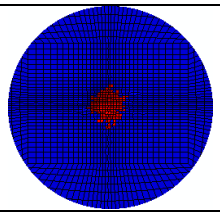	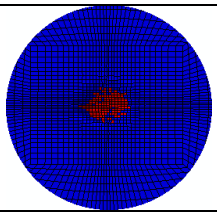	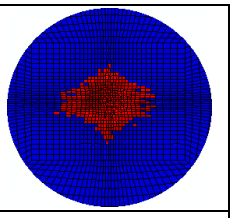
	Layer-1 (0°)	Layer-2 (45°)	Layer-3 (-45°)	Layer-4 (90°)
[30°/60°/-60°/120°]	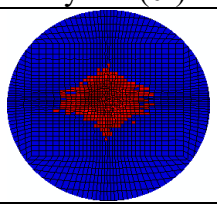	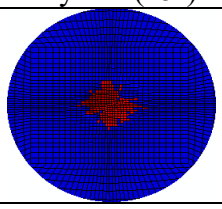	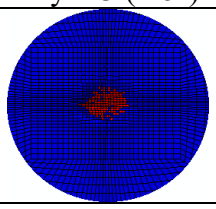	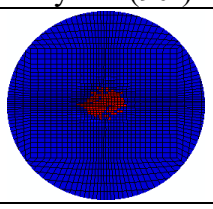
	Layer-1 (30°)	Layer-2 (60°)	Layer-3 (60°)	Layer-4 (120°)
[15°/45°/-45°/75°]	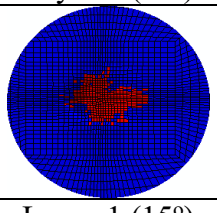	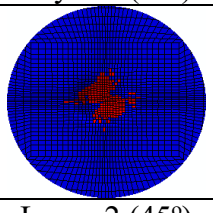	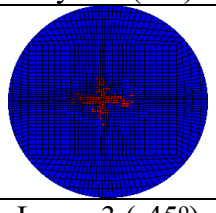	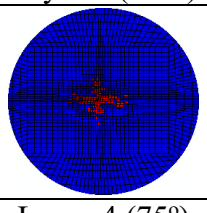
	Layer-1 (15°)	Layer-2 (45°)	Layer-3 (-45°)	Layer-4 (75°)

Figure 6: Matrix cracking at different configuration under impact energy level of 3.14 J

ISSN 1533-9211 DOI: 10.5281/zenodo.14598815

Matrix cracking occurred first in the 45° plies for the two configurations. However, in the [30°/60°/-60°/120°] laminate, cracking was more severe and propagated faster through the thickness (Fig. 6). Fiber breakage was most prominent in the 0° and 90° plies in laminates with the [0°/45°/-45°/90°] showing delayed fiber rupture compared to the [30°/60°/-60°/120°] configuration [20].

4.3.2 Cohesive Element Damage (CSDMG)

Delamination initiation and propagation are visualized in Fig. 7 using the CSDMG variable for cohesive elements. Delamination is most pronounced at the interfaces between plies with the largest angular differences, particularly between 0°/45° interface, reflecting the role of interlaminar shear stress in delamination initiation. The damage modes in angle-ply coir fiber laminates vary significantly with ply orientation and energy levels. At low energy levels, matrix cracking is the predominant mode of damage, with delamination and fiber breakage becoming more pronounced as the energy increases. Laminates with higher ply angles [30°/60°/-60°/120°] are more prone to delamination, while those with lower angles [15°/45°/-45°/75°] experience earlier fiber breakage under high impact loads. The red zones in the contour plots indicate where delamination has fully developed, leading to the separation of adjacent plies [21].

[0°/45°/-45°/90°]	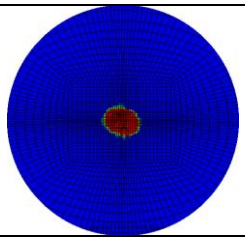	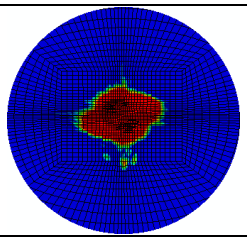	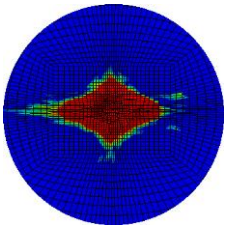
	Interface 1 (0/45)	Interface 2 (45/-45)	Interface 3 (-45/90)
[30°/60°/60°/120°]	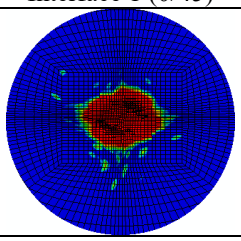	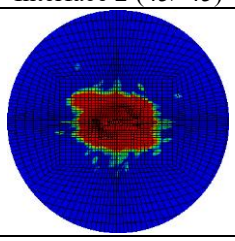	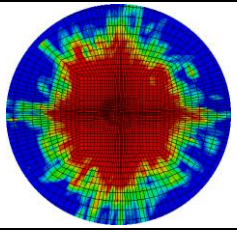
	Interface 1 (30/60)	Interface 2 (60/60)	Interface 3 (60/120)
[15°/45°/-45°/75°]	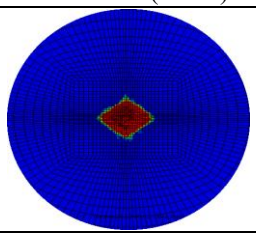	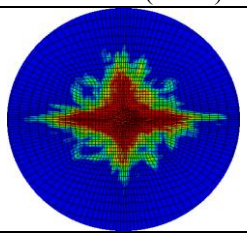	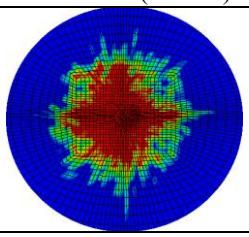
	Interface 1 (15/45)	Interface 2 (45/-45)	Interface 3 (-45/75)

Figure 7: Delamination damage at different stacking sequence of typical interfaces subjected to 15.7 J impact energy level

The Seybold Report
ISSN 1533-9211
DOI: 10.5281/zenodo.14598815

Table 2: Damage Areas for laminates and interfaces at 25 J impact energy threshold

Ply Orientation	Major delamination interface	Damage area (m^2)
[0°/45°/-45°/90°]	45°/-45°	0.0020
[30°/60°/-60°/120°]	30°/-60°	0.0025
[15°/45°/-45°/75°]	45°/75°	0.0030

As seen in Table 2, the damage area also varies significantly depending on the ply orientation. The [0°/45°/-45°/90°] laminate at same impact energy level, exhibited the smallest damage area compared to the [30°/60°/-60°/120°]. The [15°/45°/-45°/75°] configuration, in contrast, exhibited the largest damage area, reflecting its susceptibility to early failure due to less efficient stress distribution. This suggests that the [0°/45°/-45°/90°] configuration offers better protection against delamination and matrix cracking due to its superior stress distribution. The major delamination interfaces occur at plies with high angular differences, thus, 45°/-45° and 30°/60°, where the interlaminar shear stresses are highest. As impact energy increases, the damaged area expands, such as [15°/45°/-45°/75°] laminate exhibits the largest damage area for the same energy level, suggesting a lower resistance to delamination and matrix cracking than the [0°/45°/-45°/90°] laminate. The major delamination interfaces occurred at plies with significant angular differences, leading to higher interlaminar shear stresses indicating the onset of superior damage threshold [22].

CONCLUSION

This study used finite element analysis to investigate the low-velocity impact behavior of coir fiber/epoxy composite laminates, highlighting the influence of ply orientation on the material's impact performance. The results showed that ply orientation significantly affect the impact resistance, energy absorption, and failure mechanisms of the laminates. The [0°/45°/-45°/90°] configuration exhibited superior impact resistance due to more efficient stress distribution and reduced delamination. Matrix cracking and delamination were successfully captured using the Hashin-Rotem failure criterion and cohesive zone modeling, respectively. The use of cohesive zone modeling and transverse tensile stress contours provided valuable insights into the damage progression in these laminates, highlighting their potential for impact-critical applications. These findings contribute to the optimization of natural fiber composites for impact-sensitive applications.

Acknowledgements

The author would like to acknowledge all the authors for their manuscript contributions.

References

1) K. Satyanarayana, K. Sukumaran, P. Mukherjee, C. Pavithran, S. Pillai, Natural fibre-polymer composites, Publisher, City, 1990.

2) M.M. Rahman, M.F. Ramli, A.H.A. Rashid, A Review of Experimentation Numerical Simulation of Low-Velocity Impact Performances and Damages of Fiber-Reinforced Composites, Publisher, City, 2024.

The Seybold Report
ISSN 1533-9211
DOI: 10.5281/zenodo.14598815

3) H. Tuo, Z. Lu, X. Ma, J. Xing, C. Zhang, Damage and failure mechanism of thin composite laminates under low-velocity impact and compression-after-impact loading conditions, Publisher, City, 2019.

4) A. Katunin, S. Pawlak, A. Wronkowicz-Katunin, D. Tutajewicz, Damage progression in fibre reinforced polymer composites subjected to low-velocity repeated impact loading, Publisher, City, 2020.

5) B. Sozen, T. Coskun, O.S. Sahin, Dynamic characterization and damage analysis for the thermoplastic fiber-reinforced epoxy composites exposed to repeated low velocity impact, Publisher, City, 2024.

6) M.Z. Khan, S.K. Srivastava, M. Gupta, Tensile and flexural properties of natural fiber reinforced polymer composites: A review, Publisher, City, 2018.

7) A. Veerasimman, V. Shanmugam, S. Rajendran, D.J. Johnson, A. Subbiah, J. Koilpichai, U. Marimuthu, Thermal properties of natural fiber sisal based hybrid composites–a brief review, Publisher, City, 2022.

8) M. Sanjay, P. Madhu, M. Jawaid, P. Senthamaraikannan, S. Senthil, S. Pradeep, Characterization and properties of natural fiber polymer composites: A comprehensive review, Publisher, City, 2018.

9) N. Nurazzi, M. Asyraf, S. Fatimah Athiyah, S. Shazleen, S.A. Rafiqah, M. Harussani, S. Kamarudin, M. Razman, M. Rahmah, E. Zainudin, A review on mechanical performance of hybrid natural fiber polymer composites for structural applications, Publisher, City, 2021.

10) T.K. Khieng, S. Debnath, E. Ting Chaw Liang, M. Anwar, A. Pramanik, A.K. Basak, A review on mechanical properties of natural fibre reinforced polymer composites under various strain rates, Publisher, City, 2021.

11) M. Kozlov, S. Sheshenin, Modeling the progressive failure of laminated composites, Publisher, City, 2016.

12) J. Wei, L. Sun, X. Gao, W. Huang, Microstructures failure analysis of fiber reinforced composites with various void types, Publisher, City, 2023.

13) S. Long, X. Yao, X. Zhang, Delamination prediction in composite laminates under low-velocity impact, Publisher, City, 2015.

14) A. Version, 6.11. User's manual, Publisher, City, 2011.

15) A.U.s. Manual, Version 6.11, Publisher, City, 2011.

16) N. Gayathri, V. Shanmuganathan, A. Joyson, M. Aakash, A.G. Joseph, Mechanical properties investigation on natural fiber reinforced epoxy polymer composite, Publisher, City, 2023.

17) Y. Shi, T. Swait, C. Soutis, Modelling damage evolution in composite laminates subjected to low velocity impact, Publisher, City, 2012.

18) M.S. Siddiqui, M. Rabbi, S. Dewanjee, Low-velocity impact response of natural fibre reinforced composites: a comprehensive review on influential parameters, Publisher, City, 2023.

19) V.S. Anuse, K. Shankar, R. Velmurugan, S.K. Ha, Compression-After-Impact analysis of carbon fiber reinforced composite laminate with different ply orientation sequences, Publisher, City, 2022.

20) M.S. Moreno, S.H. Muñoz, Mechanical response of±45° angle-ply CFRP plates under low-velocity impact and quasi-static indentation: Influence of the multidirectional strain state, Publisher, City, 2020.

21) M.K. Singh, R. Kitey, Enhancing low velocity impact characteristics of glass fiber laminates by short fiber reinforcement—Failure evolution and damage mechanisms, Publisher, City, 2022.

22) T. Bian, Q. Lyu, X. Fan, X. Zhang, X. Li, Z. Guo, Effects of fiber architectures on the impact resistance of composite laminates under low-velocity impact, Publisher, City, 2022.